Design and Evaluation of a Robotic System for Transcranial Magnetic Stimulation

Lucile Zorn, Pierre Renaud*, Bernard Bayle, Laurent Goffin, Cyrille Lebossé, Michel de Mathelin, and Jack Foucher

***Abstract*—Transcranial magnetic stimulation is a noninvasive brain stimulation technique. It is based on current induction in the brain with a stimulation coil emitting a strong varying magnetic field. Its development is currently limited by the lack of accuracy and repeatability of manual coil positioning. A dedicated robotic system is proposed in this paper. Contrary to previous approaches in the field, a custom design is introduced to maximize the safety of the subject. Furthermore, the control of the force applied by the coil on the subject's head is implemented. The architecture is original and its experimental evaluation demonstrates its interest: the compensation of the head motion is combined with the force control to ensure accuracy and safety during the stimulation.**

***Index Terms*—Force control, medical robotics, robot design and control, transcranial magnetic stimulation (TMS).**

I. Introduction

TRANSCRANIAL magnetic stimulation (TMS) is a noninvasive method to deliver electric stimulation to the cortex. The stimulation results from a rapidly changing magnetic field generated with an external coil (see Fig. 1) that goes through the skull and induces electric currents in the brain. TMS has been used in clinical and neurological studies for more than 25 years [1]. More recently, single pulse and repetitive TMS have been applied in clinical research for the treatment of neurological and psychiatric diseases. The efficiency of TMS has been demonstrated in the case of depression [2], [3]. Its effect on several other pathologies, such as compulsive obsessive disorders, schizophrenia, or posttraumatic stress disorders, is currently being investigated [4], [5]. This promising technique has been approved in the U.S., Canada, and Israel for patients whose antidepressant medication has failed. However, it is not yet widely accepted because its efficiency varies substantially between subjects.

Manuscript received July 28, 2011; revised October 8, 2011; accepted November 20, 2011. Date of publication December 15, 2011; date of current version February 17, 2012. This work was supported by the Region Alsace and the Agence Nationale de la Recherche through the EmergenceTec program. *Asterisk indicates corresponding author.*

L. Zorn, B. Bayle, L. Goffin, and M. de Mathelin are with the Laboratoire des Sciences de l'Image, de l'Informatique et de la Télédétection, CNRS, University of Strasbourg, 67091 Strasbourg, France (e-mail: lucile.zorn@lsiit-cnrs.unistra.fr; bernard.bayle@unistra.fr; laugof@gmail.com; demathelin@unistra.fr).

*P. Renaud is with the Institut National des Sciences Appliquées, 67084 Strasbourg, France, and also with the Laboratoire des Sciences de l'Image, de l'Informatique et de la Télédétection, CNRS, University of Strasbourg, 67091 Strasbourg, France (e-mail: pierre.renaud@insa-strasbourg.fr).

C. Lebossé is with Luxscan Technologies, 4384 Ehlerange, Luxembourg (e-mail: cyrille_lebosse@yahoo.fr).

J. Foucher is with the Department of Psychiatry, University Hospital of Strasbourg, 67098 Strasbourg, France (e-mail: jack.foucher@laposte.net).

Color versions of one or more of the figures in this paper are available online at http://ieeexplore.ieee.org.

Digital Object Identifier 10.1109/TBME.2011.2179938

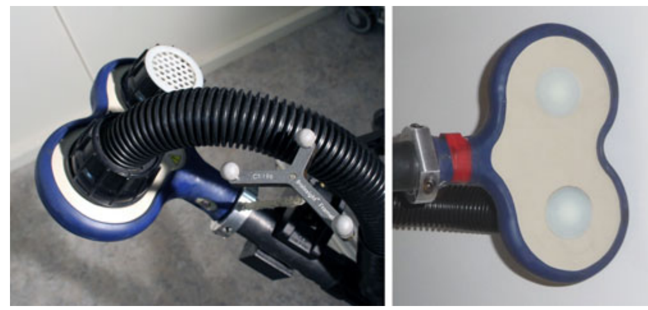

Fig. 1. Top and bottom views of a figure-of-eight stimulation coil.

Fig. 2. TMS setup with localizer for navigation.

The variability is partially due to how the stimulation gesture is performed [6], [7]. Up to now [8], [9], the most accurate method has been to position the coil manually with the help of a navigation software [10], [11]. This tool combines preoperative MR images and peroperative data from an optical localizer (see Fig. 2) in order to display in a graphical interface the actual position of the coil with respect to the subject's brain. Even with such an assistance, it remains difficult to obtain an accuracy of a few millimeters in a repeatable manner. The main reason is that each procedure lasts more than 30 min with a coil that weighs more than 2 kg. A static positioning system is sometimes used to hold the coil (see Fig. 2). In such a case, it is not possible to follow continuous trajectories nor to compensate for involuntary motions of the subject during the session.

Robotic assistance will allow us to evaluate the benefits of TMS in a more adequate manner, certainly leading to a faster development of this technique. The initial positioning of the stimulation coil will be simplified and the coil position will be tracked in presence of subject movements. Some early experimental results of robotized TMS have been reported on phantoms [12] and healthy subjects [13]. They confirm the interest of robotization to improve stimulation accuracy. However, in these studies, the force applied by the robot on the subject's head is not used for the robot control nor even measured and supervised. The lack of contact control has two main disadvantages. First, it is responsible for air gaps between the subject's head and the coil that lower the magnetic induction and then the treatment efficiency. More importantly, it constitutes a major limitation in terms of safety.

Recently, a robotic setup has been proposed that includes an industrial force sensor between the robot end-effector and the stimulation coil [14]. The system is based on an industrial anthropomorphic robot, with a drastically different workspace from the one required for the application, i.e., roughly the upper half head. In addition, like any industrial robot, the system is equipped with actuators selected for high-speed motions, which should be avoided for such an application where the robot is very close to the subject. The use of this kind of robot architecture contradicts the principles of intrinsically safe robots [15], [16] since the designer cannot ensure at the hardware level that the device will not become harmful for the subject. The safety only relies on software programming to avoid potential risks.

In our opinion, safety requirements can be improved with regard to the early works on robotized TMS. To that purpose, we have proposed to develop a dedicated robotic system for TMS [17], [18]. In this paper, we introduce this robotic system, detail the design of its architecture and the control strategy, and evaluate its performances. Its design and control optimize the safety of the procedure. In particular, the force applied by the robot on the head is controlled. The movements of the head are also compensated in order to ensure the accuracy of the procedure throughout the session. The paper is organized as follows. The workflow of robotized TMS is presented in Section II. The requirements for the robotic system and the resulting specifications are introduced in Section III. The mechanical design of the proposed system is described in Section IV. Then, the robot planning and control are detailed in Section V. The experimental evaluation of the system is developed in Section VI to demonstrate its interest for the development of TMS. Finally, conclusion and perspectives are given in Section VII.

II. Workflow

The proposed robotized TMS procedure results from the adaptation of conventional navigated TMS, as summarized in Fig. 3. The preoperative phase starts with the acquisition of MR images of the subject to reconstruct the brain and the head after segmentation. Characteristic anatomical landmarks are pointed in the images in order to register the head with the preoperative medical images during the stimulation session. Then, the neurologist plans the treatment, which corresponds to continuous trajectories or to a simple list of points on the brain. This medical planning can be performed in different ways. The anatomical images can be used alone or after coregistration of additional information provided for instance by fMRI or PET. A pilot TMS session can also be used to determine target positions. After the planning, the reference trajectory on the head is computed.

The peroperative procedure begins with the subject registration. The subject wears glasses equipped with a marker, i.e., a set of fiducials, so that the head position and orientation can

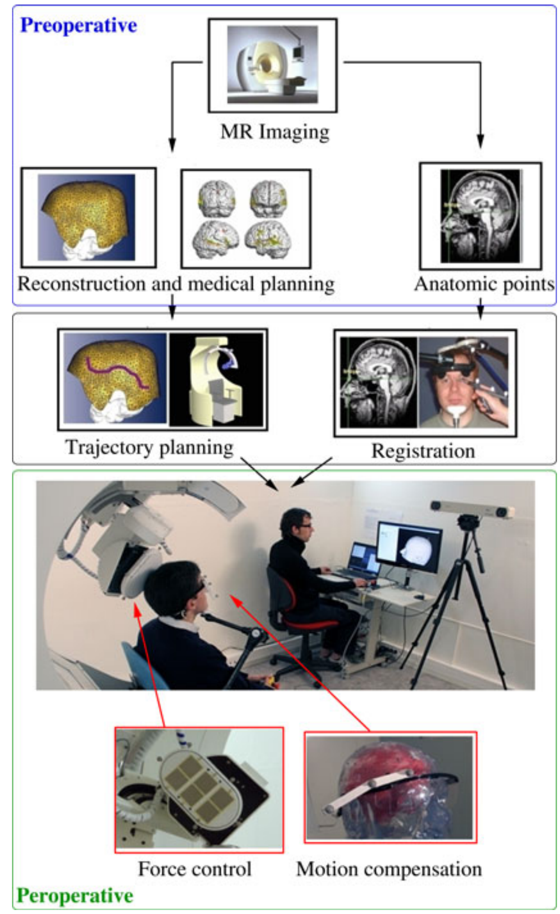

Fig. 3. Workflow of robotized navigated TMS.

be measured by an optical localizer (NDI Polaris [19]). The anatomical landmarks are pointed on the subject's head to register its position with respect to the medical images and also to determine its position with respect to the robot reference frame. The subject is, then, moved using a mobile seat to place properly the head with respect to the robot workspace. Superior-inferior and antero-posterior movements are provided to position correctly the subject. At that time, the reference trajectory of the coil on the head is computed in the robot frame and the corresponding trajectory for the robot joints is planned. Once the registration and planning steps have been achieved, the treatment itself begins. During the stimulation, the head motion is tracked and compensated by the robot using the marker on the subject's glasses, while the force applied by the coil on the head is controlled.

III. System Requirements

A. Coil Positioning

Most widespread stimulation coils have a figure-of-eight shape with a planar surface of contact (see Fig. 1). The current induction in the brain has been described by several models [20]–[22]. They consistently state that the brain tissue is maximally excited along the line that is orthogonal to the contact plane and goes through the coil center (see Fig. 4).

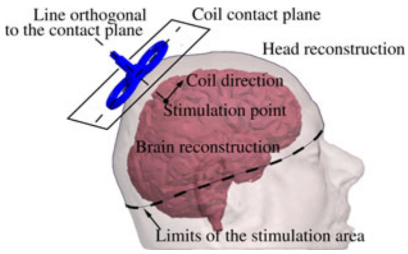

Fig. 4. Constraints of the stimulation coil positioning.

The orientation of the coil is also important. The cortical response is indeed maximal when the longitudinal axis of the coil is parallel to the cortical columns [21], an anatomical structure that is identified in the medical images. The excitation decreases as a function of the square of the distance to the coil, with a significant stimulation effect in the first 1.5–2 cm of the head [23], [24]. The stimulation is dramatically reduced if any air gap exists between the coil and the head. Finally, the coil position and orientation are defined by three constraints (see Fig. 4). First, the line orthogonal to the contact plane going through the coil center must intersect the point to be stimulated. Second, the coil contact plane must be tangent to the head. Third, the coil self-rotation is required and any value should be reachable.

From a robotic point of view, the positioning of the coil is a 6-degree-of-freedom task. Additionally, the center of the coil has to remain in an area covered by the hair as well as the forehead and the temples. For safety and comfort reasons, the force applied by the stimulation coil on the head must remain limited, around 3 N to 5 N, from experimental estimations. To improve the comfort, the head may also be supported by an external device such as the chin support represented in Fig. 3. Even with such a device, the position of the subject can slowly vary of a few centimeters during a session and these movements have to be compensated.

B. Medical Requirements

TMS is an external procedure. Sterilization is, therefore, not required. The magnetic field necessary for the stimulation reaches 1 to 2 T in approximately 100 ms [25]. It is responsible for an electric field with peak values up to 600 V/m. An experimental evaluation was performed with the custom-made coil integrated in the robotic system. In that case, the magnetic induction is significant for active elements or ferromagnetic components within a 60-mm distance from the coil center [26].

IV. Mechanical Design

A. Kinematic Decomposition

We propose to decompose the robotic task in three subtasks as illustrated in Fig. 5, in order to design a robot whose workspace is very similar to the one required by the TMS task. The first subtask consists in positioning the coil around the head as represented in Fig. 5(a), by rotating around the head center.[1] The second subtask consists in rotating the coil to ensure tangency with the head as well as a correct orientation [see Fig. 5(b)]. The third subtask consists in ensuring the contact between the coil and the head as illustrated in Fig. 5(c).

[1]The "head center" is determined from the anatomical landmarks.

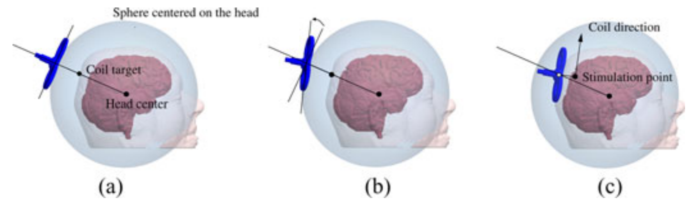

Fig. 5. Decomposition of the robotic task. (a) Positioning. (b) Orientation. (c) Contact.

B. Mechanism Synthesis

The proposed robotic system is designed in order to achieve these three subtasks by means of three subsystems: a spherical arm, a prismatic joint, and a spherical wrist. The synthesis of these subsystems is described hereafter. Head geometry varies between subjects. As a consequence, six different head reconstructions were used during the design in combination with anthropometric data issued from [27] and [28].

1) Synthesis of the Spherical Arm:

a) Mechanism type synthesis: The arm aims at positioning the coil center around the head. Because of the head geometry, a spherical robot seems the most adequate architecture to reach any point of the task workspace. Even though spherical parallel [29] or hybrid [30] architectures have been proposed in the literature, a serial architecture is preferred for its better size/workspace ratio. The most simple spherical serial architecture is obtained with two revolute joints, designated as R joints in the following. The RR mechanism that best fits the task workspace is composed of two links with 90° arc lengths, connected by R joints whose axes intersect at the center of rotation. Since the task workspace is slightly larger than a hemisphere, it is however not possible to reach any point. In other words, an RR mechanism would lack versatility and would limit the achievable stimulation protocols. Additionally, the fully extended and fully folded configurations are singular. A redundant arm of type RRR is, therefore, chosen. The spherical RRR mechanism (J1-J2-J3 in Fig. 6) is fully defined by the arc lengths of its links and the position of the first R joint axis with respect to the head. These parameters have now to be selected.

b) Isotropy analysis: In the first step, the kinematic behavior of the mechanism is analyzed by considering the evolution of the isotropy index [31] over the task workspace. From this analysis, it is possible to determine the importance of the robot architecture on the behavior of the robotic system, before selecting a mechanism. The isotropy index varies between 0 in the case of a kinematic singularity and 1 when the mechanism can move equally in any direction. A set of possible architectures is generated by considering the following:

1) three different positions of the first joint axis with respect to the head: on the side, above, or behind the head;
2) a sum of the arc lengths greater or equal to 210° to ensure that every point of the workspace is reachable;

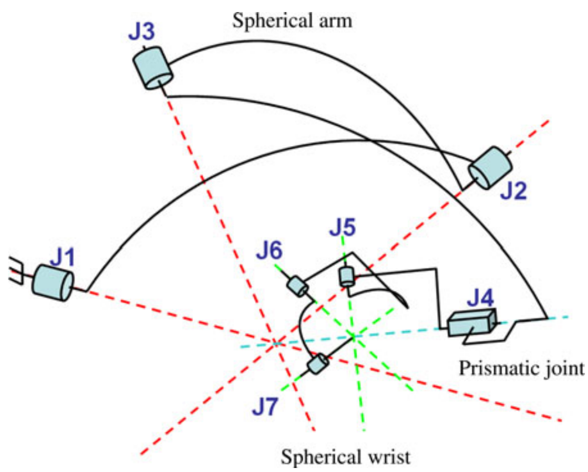

Fig. 6. Kinematic scheme of the mechanism, including the arm, the prismatic joint, and the wrist [18].

Fig. 7. Robotic system.

3) a maximum arc length equal to 90°, to limit the flexibility of the links. For the same reason, the length of a link is chosen smaller than the one of the link on which it is mounted.

Arc lengths are discretized with a 10° step, and the task workspace is discretized in 325 points. For each point, the mechanism configuration is determined by optimizing the isotropy index thanks to the manipulator redundancy [32]. The analysis of the system isotropy for the resulting 3×23 parameters combinations outlines that the kinematic behavior is not strongly dependent on the mechanism geometry. The average value of the isotropy index over the task workspace varies by less than 17%. Among the possible choices, the 90°/90°/90° mechanism is of particular interest: its kinematic behavior is satisfactory and it can be designed using links of circular shape combined with R joints but also with circular guides, denoted as CG in the following. These latter are guides whose shape allows us to obtain a circular motion with an improved stiffness compared to an R joint associated to a circular structure element.

c) Selection of the joint types and the mechanism position: A second analysis is achieved to choose between R and CG joints for the joints of the spherical arm. A CG joint is preferred for the first joint to improve the mechanism stiffness. It is positioned in the vertical plane to limit the surface on the ground. The mechanism that drives the carriage on the circular guide can then be positioned behind the subject. For the two other joints, at least one CG has to be used to limit the flexibility. The CG-R-CG architecture is the most interesting solution, in particular, because interferences between the mechanism and the subject can be avoided by defining simple joint limits. Actually, two out of the three joint limits can be defined at the hardware level, which gives a high level of safety.

2) Synthesis of the Prismatic Joint: The only issue for the second subsystem (J4 in Fig. 6) is the joint range needed to fulfill the task requirements. It is determined from anthropomorphic measurements [28], [33] that a 80-mm translation allows us to treat more than 95% of adults. The number of subjects for whom robotized stimulation may be only partially achievable is, therefore, considered acceptable.

3) Synthesis of the Wrist: The wrist is necessary to ensure the coil tangency with the head, since the head is not exactly a sphere and the head center cannot be supposed to be perfectly superimposed with the spherical arm center. The required angular ranges of the wrist joints (J5-J6-J7 in Fig. 6) increase when the head geometrical center and the spherical arm center are moved away from each other. As a consequence, the subject position is set initially using the mobile chair to minimize the distance between the head and the mechanism centers. The angular amplitudes are determined from the reconstructed head models, taking into account subject positioning errors equal to 50 mm due to the initial positioning and the subject movements during the stimulation.

For compactness and rigidity sake, the wrist is also designed using a combination of R and CG joints. The CG-CG-R architecture is selected, since it allows us to have free space at the wrist center of rotation to integrate the coil. The remote center of motion obtained with this arrangement also simplifies the control: the wrist modifies the coil orientation without affecting the coil center position.

C. Design Choices

1) General Structure: The system is composed of the robot and the mobile seat. Its overall volume is 0.75 m × 1.4 m × 1.9 m and its weight is approximately 400 kg. The prototype of the system is pictured in Fig. 7. The power, velocity, and maximum torque of the actuators are voluntarily limited to optimize the safety of the device.

The actuation power of the prismatic joint is for instance limited to 6 W and the maximum coil velocity due to its translation is of 6 mm/s to fit the task requirement. The overall CAD view is given in Fig. 8. Some details on cable management are removed for sake of clarity. The three subsystems (see Figs. 9–11) are described in the rest of this section to emphasize the safety features.

2) Arm: The actuation of J1 is performed by a transformation mechanism (see Fig. 8). A direct current motor rotates a ball screw which translates one end of the connecting rods that are

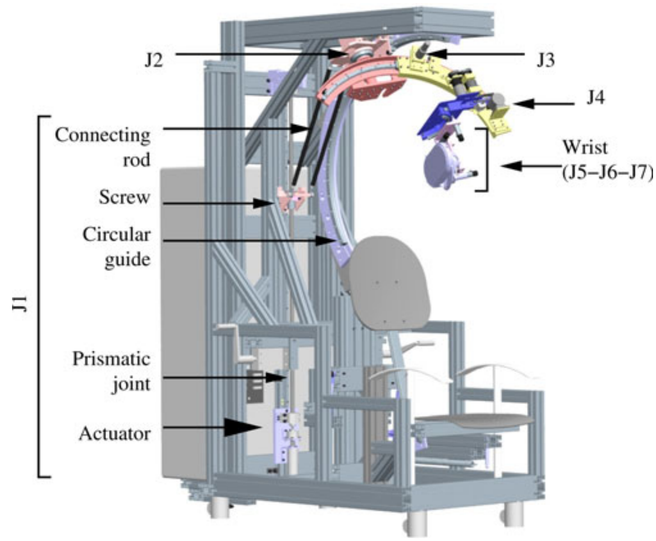

Fig. 8. CAD view of the robotic system without enclosure.

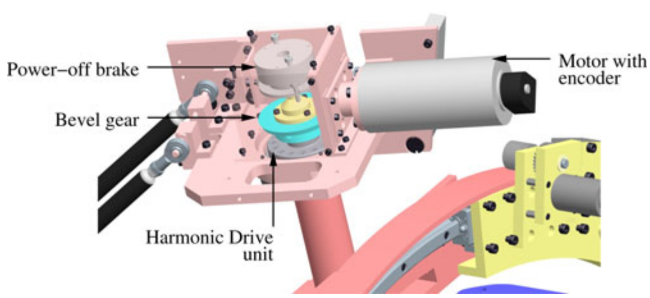

Fig. 9. Close-up on the joint J2.

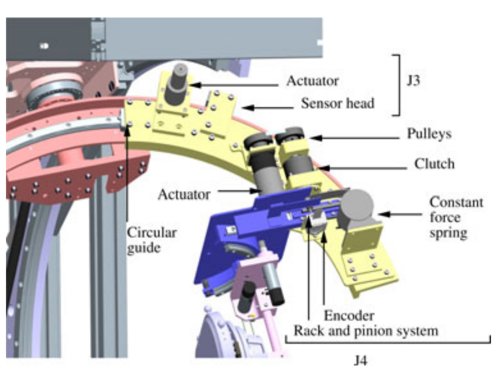

Fig. 10. Close-up on the joints J3 and J4.

linked at their other end to the carriage moving on the circular guide. The system is not backdrivable. Its configuration allows us to minimize the global size of the device as the ball screw is located vertically behind the subject.

The joint J2 (see Fig. 9) is based on a harmonic drive gear unit and a power-off brake. A direct current motor actuates the gear unit thanks to a bevel gear. Contrary to the joints J1 and J3, safety is here obtained by having a backdrivable joint. If a

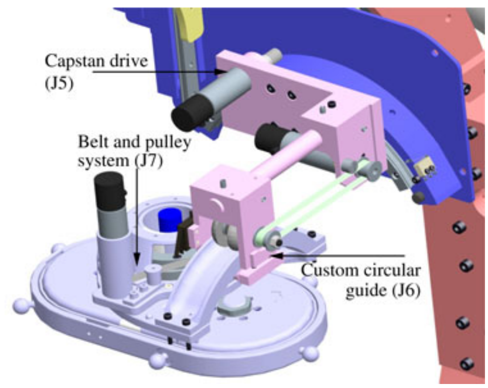

Fig. 11. Close-up on the wrist.

power failure occurs, or in case of emergency, the power-off brake mounted in parallel stops and maintains the robotic arm in a static position. To help the subject exit the system, the power-off brake can be momentarily disabled by the operator and the arm can, then, be rotated manually as the gear unit is backdrivable.

The redundancy of the arm can be used in different ways. For several protocols, such as the cartography of the motor cortex area, a satisfactory behavior can be obtained by determining initially the most adequate joint value for J3, that will remain constant during the stimulation. For other protocols, a continuous variation of the joint is needed. Two alternate designs are, therefore, considered. The first design corresponds to a continuous variation of J3. It is based on a cable transmission (see Fig. 10), using the principle of a capstan drive. A pulley is mounted on the motor. A cable is fixed at its ends to the element to be displaced and winded around the actuated pulley. The rotation of the pulley creates the rotational movement of the element connected to the circular guide. To avoid the introduction of any bias due to some sliding of the cable, an independent and direct measurement of the angular position is performed using an optical ruler. The second design is a simplified design. A discrete set of positions is available by manually moving the axis. This is the version implemented in the first prototype of Fig. 7.

3) Prismatic Joint: For the joint J4, passive safety is obtained by a constant force spring placed in parallel to the joint actuation (see Fig. 10). It tends to pull the wrist outwards the subject's head so that the motor is constantly acting against this spring. In case of a power failure or an emergency, the motor is disconnected with a clutch and the spring automatically removes the coil from the head. The clutch is mounted with its axis parallel to the motor axis to maximize the compactness. The actuator rotation is converted into a translation of the wrist using a rack and pinion system.

4) Wrist: The wrist (see Fig. 11) is close to the magnetic field generated by the stimulation coil. The presence of ferromagnetic elements is, therefore, as reduced as possible. Most structural elements are manufactured using rapid prototyping techniques with polymer materials. A custom-made compact CG joint is designed for the joint J6, whose motion results from the rotation of a roller guided by a circular guide connected to the coil. Capstan drives are used for the joints J5 and J6, whereas a belt

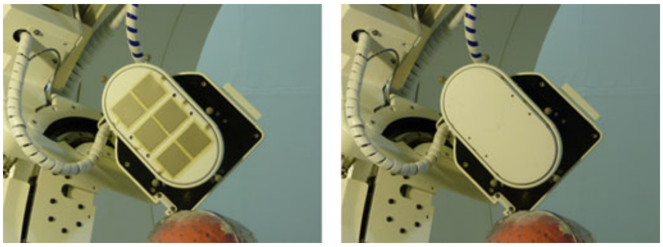

Fig. 12. (Left) Array of six force sensors to measure the contact force. (Right) Mechanical interface to measure the contact force on the whole coil surface.

and pulley transmission is chosen for the joint J7. A set of six piezoresistive force sensors [34] is embedded in the coil casing and placed beneath a thin plastic sheet in order to measure the force over the whole coil surface (see Fig. 12). The contact force can be measured directly because of the insensitivity of the sensors to the magnetic field and their very small thickness that limits the distance between the coil surface and the head.

V. Registration, Planning, and Control

A. Subject Registration

The TMS session starts when the subject sits down on the mobile seat of the robotic system. The first step is the registration of his head with respect to the robot and the reconstructed head model. As already evoked in Section II, the registration of the head with respect to the reconstructed head model is performed using a landmark matching method. Once the anatomical landmarks have been pointed in the medical images, a Polaris pointer is used to designate three or four of them on the head, typically the tragus of the left and right ears, the bridge of the nose, and the nasal tip. Then, a point-to-point correspondence is performed, based on a least-squares minimization method [35]. Registration accuracy is not affected by head motions during the landmark acquisition, since each acquired point is recorded in the frame associated with the marker attached to the subject glasses. The registration of the head with respect to the robot frame is achieved by using another marker attached to the base of the mechanism.

The registration procedure can induce translation and orientation errors. Their influence on the accuracy of the stimulation process is not easy to estimate. The accuracy is dependent on the user and on the location of the stimulation points. The considered procedure is the most frequently used by clinicians performing TMS with a navigation system based on a Polaris device. We, therefore, assume that the registration accuracy provided by this technique is acceptable and we will not investigate it any further in this paper. Other techniques based on surface matching [36] instead of point matching could, however, be considered in future developments.

B. Planning

1) Reference Motion Computation: The path of the coil is computed from the positions of the targets on the cortex by considering two constraints expressed in Section III: 1) the line normal to the coil plane and going through the coil center also goes through the cortical point; and 2) the distance between the coil center and the cortical point is minimal. For each point, the facet of the reconstructed polyhedral head whose normal and center are the closest to the target point is searched for. The search is limited to the part of the model corresponding to the treatment area. In a second step, a cubic spline-based interpolation is performed between the obtained points in order to get a smooth reference path. Finally, the coil path is sampled and the reference velocity at each sampled point is derived from the stimulation frequency and the imposed number of pulses per stimulation point defined by the neurologist. For some procedures, the stimulation is limited to a discrete set of points. In this case, only the first step of the planning process is required.

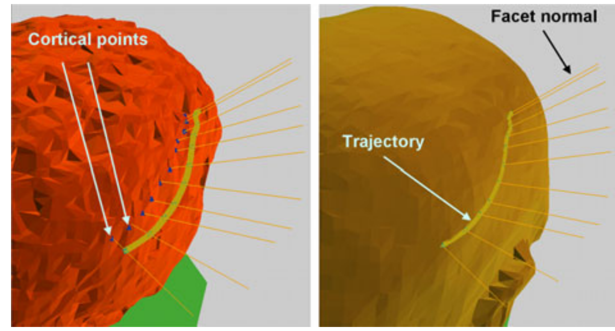

Fig. 13. (Left) Brain with the cortical points. (Right) Head model with the closest facet normals and the computed trajectory.

An illustration of the planning process is given in Fig. 13. The overall error generated by the planning, which depends on the 3-D model resolution, is estimated around 0.5 mm.

2) Robotic Motion Planning: If the joint J3 is actuated manually, there is no kinematic redundancy during the stimulation session. In that case, it is only necessary to compute the value of the joint J3 to obtain a motion for which every point is reachable and the joint positions and velocities are admissible. The joint positions are chosen as far as possible from their limits to allow the nonplanned compensation of head movements.

A robotic planning technique has been developed for the case of a continuous actuation of J3. The planning problem is highly constrained, with constraints on the joint positions and velocities. The proposed planning technique is based on probabilistic motion planning algorithms [37]. A roadmap is formed by an iterative building of a graph of randomly generated robot configurations [38]. Each configuration corresponds to a pose of the coil on the reference path. The proposed technique, detailed in [18], includes in an original manner the velocities constraints in the roadmap at the planning level which allows for instance joint limit avoidance.

C. Control

1) General Structure: The overall control structure of the system is represented in Fig. 14. It is composed of two feedback control loops: one for the force control of the joint J4 and the other for the position control of the other joints.

2) Position Control Head Motion Compensation: The control of all the joints except J4 is a conventional Cartesian control,

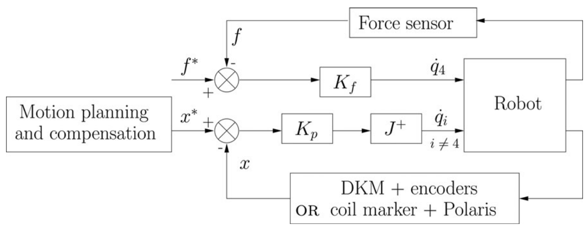

Fig. 14. Architecture of the robot control.

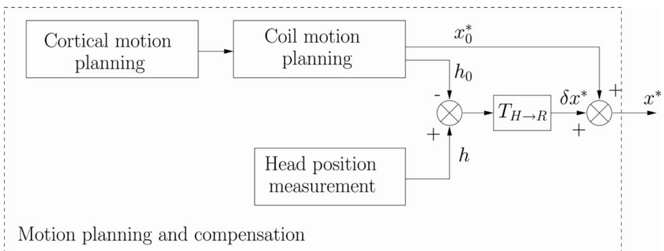

Fig. 15. Motion planning and compensation.

for which the reference motion is given by the desired coil position vector x^* (including orientation), obtained in the motion planning and compensation process, described hereafter. It requires the inversion of the robot Jacobian J, and it is tuned by a simple gain K_p. The robot pose x necessary for feedback is evaluated from the direct kinematic model (DKM) and the joint configuration q measured by the encoders. Note that it could also be obtained using the Polaris and a marker attached to the coil (see Section VI).

The motion x_0^* planned for the initial position h_0 of the head cannot be directly executed due to unavoidable head movements, which impose to modify the coil reference motion. For this reason, it is necessary to continuously evaluate the joint velocity shift that has to be applied to compensate for head motions. This is the role of the "Motion planning and compensation" block in Fig. 14. It operates as follows (see Fig. 15). Head position is supervised using the Polaris and the marker on the subject's glasses. The changes in the subject's head position are calculated by comparing the initial position h_0 with the actual position h. Then, this difference is computed relative to the robot, using the transformation matrix $T_{H\to R}$ between the head and robot frames. The resulting corrective term δx^* is added to the initially planned position x_0^*, so that the coil may follow the specified motion relative to the head.

Robot dynamics are limited for safety purpose, and fast motions of the head are, therefore, not compensated. In case of sudden subject movements, the robot will stop and wait for the operator to start the process again.

3) Force Control: Joint J4 is the only force controlled joint. Before the stimulation, the joint is in its upper position so that the coil remains as far as possible from the head while the spherical arm is moving. When the stimulation is about to begin, the joint is slowly moved in the direction of the head, with a temporary velocity control of the joint. As soon as the contact between the coil and the head is detected, the robot stops and the direct force control of the joint is started. A proportional

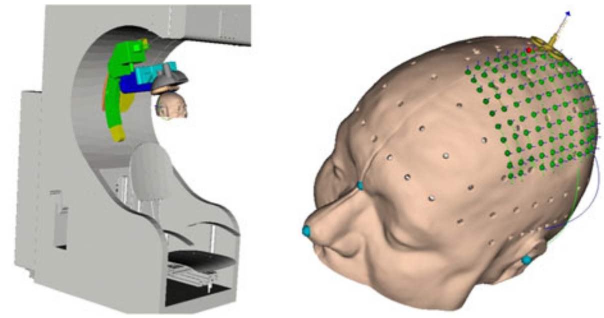

Fig. 16. Two snapshots of the supervision HMI. (Left) Overall view to check for preplanned motions and subject placement. (Right) Closeup on the task, here a grid of points to be reached. The scale of the coil is then reduced in order to improve the visualization of the task.

control is used, which is tuned by the gain K_f (see Fig. 14). The reference force f^*, which corresponds to a light pressure on the head, is compared to the force f measured by the piezoresistive sensors. In case of fast head motions, the contact with the coil may be interrupted. Then, the robot force control is stopped, as previously done in the case of motion compensation.

One peculiar feature of the implemented robot force control is its sensing technology. Interlink force sensing resistor (FSR) piezoresistive sensors have been selected for the implementation of the force control [34].

Six of them are connected in parallel to detect any interaction with the head, independently from the contact point, though this latter is supposed to be always centered. The FSR sensor which is originally dedicated to contact detection proves efficient to solve the delicate problem of force sensing given the demanding specifications of the system.

D. Software

1) Controller: The robot controller is implemented using Adept SmartMotion modules (SMI6). The real-time software includes all the necessary protections to operate with a high level of safety. An application programming interface allows the launching of real-time tasks and status checking or measurements from a supervision software. The stimulation is also driven by the low level software, using the trigger input of the stimulator.

2) Supervision: The supervision software, which is not real time, runs on a notebook PC. It is designed to manage all the preoperative procedures and to supervise the stimulation process. The notebook used in our experiments has an Intel Core 2 Duo processor, at 2.8 GHz. The software programmed in C# runs under Windows environment. It uses the 3-D visualization toolkit for visual rendering (see Fig. 16). The supervision software is connected to the Polaris localizer by a serial link and to the robot controller by an IEEE 1394 link.

This supervision software is used at every step of the robotic planning. At the beginning of the procedure, it helps positioning the subject by optimizing the head position and the robot accessibility. During the stimulation, the program supervises the head motions using a nonreal-time supervision at 10 Hz, well beyond the frequency of the motions to be compensated. It also computes the corrections applied to the reference motion.

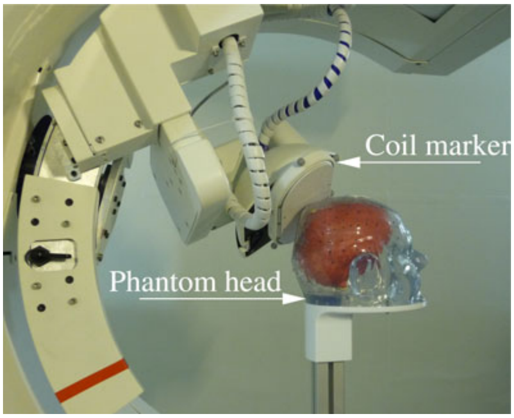

Fig. 17. Phantom head during experimental evaluation of the system accuracy.

VI. Experimental Evaluation

The experimental evaluation is performed using a phantom composed of a head and a brain mock-ups (see Fig. 17). They are reconstructed from MR images and manufactured using rapid prototyping techniques.

The Polaris is used to evaluate the system performances. To do so, the coil casing is equipped with a marker composed of six fiducials (see Fig. 17). Only three of them need to be observed simultaneously by the Polaris to compute the position and the orientation of the coil. The measurement can, therefore, be performed independently from the coil rotation. The Polaris accuracy is in the order of 0.25 mm, with a measurement rate of 30 Hz and a time drift estimated to be equal to 0.3 mm in 30 min, the average duration of the presented experiments.

Three features are considered in the evaluation: stimulation accuracy without head movements, compensation of the head movement, and force control. Experimental procedures and results are introduced before discussing the robotic system performance.

A. Stimulation Accuracy

This evaluation is performed by analyzing first the repeatability of the coil positioning, i.e., the coil position variation under constant conditions, and then the positioning error which is the difference between the planned stimulation point and the point that is finally reached.

1) Repeatability: The repeatability of the stimulation process is dependent on the repeatability of the head registration, the measurement of the head position, and the robotic system. As outlined in Section V-A, the head registration is performed with the method currently used in the manual procedures. The localization system is similar to the one generally used in manual procedures. Then, it is interesting to focus on the evaluation of the robotic system repeatability.

The coil is positioned ten times along a regular grid of 50 points projected on the head. With current stimulation systems, the depth of stimulation does not exceed 25 mm. Repeatability is, therefore, assessed for a point located 25 mm below the stimulation coil along the perpendicular line that goes through the coil center. The average standard deviation, used here to estimate the repeatability, is equal to 0.4 mm with a maximum standard deviation in the robot workspace equal to 0.7 mm.

TABLE I
Mean Positioning Errors

Control strategy	Mean normal error (mm)	Mean tangential error (mm)
Open loop	2.7	5.0
Closed loop	2.5	0.6
Open loop with correction	2.4	2.1
Open loop with correction after head movement	2.8	2.6

2) Positioning Error: A set of 75 points equally distributed around the stimulation area on the phantom head is defined. The stimulation coil is positioned on each of them, using the force control for the joint J4. For each point, an error vector is computed by comparing the actual and planned positions of the point located 25 mm below the stimulation coil. This vector is then projected in the plane of the coil and along its perpendicular to evaluate, respectively, the so-called tangential and normal errors. A normal error affects the stimulation intensity, whereas a tangential error represents an error in the selection of the stimulated area.

A first control strategy consists in using the DKM (see Section V-C2), in a so-called open-loop control strategy. The mean error values over the set of 75 points are reported in Table I, line 2.

For a significant portion of the workspace, the position of the coil can be measured thanks to the coil marker and the Polaris. A second strategy consists, therefore, in a closed-loop control based on this measurement. The corresponding results are reported in line 3 of Table I. In that situation, the positioning error is no longer dependent on the kinematic model of the robot.

The subject can create total occlusions of the coil marker. In such a case, the closed-loop strategy is no longer possible. A third control strategy is, therefore, introduced to take advantage of the closed-loop control that can be achieved in the absence of the subject. The procedure is composed of two steps. In a first step, the closed-loop control is used to position the coil along the predefined set of points. The joint J4 is then position controlled. The closed-loop control allows us to determine the joint corrections needed to compensate for the positioning errors. Those joint corrections are introduced in a second step, with an open-loop control of the robot in presence of the subject. The corresponding results are indicated in Table I when the head and mechanism centers are superimposed (line 4) and when a 15-mm displacement of the head is voluntarily introduced to assess the robustness of the trajectory correction (line 5).

B. Motion Compensation

The efficiency of the motion compensation is evaluated by displacing voluntarily the phantom head with the seat. The degrees of freedom of the seat differ from those of the robot. In other words, the compensation of a seat movement, even if it consists in a pure translation, requires the simultaneous control of all the robot joints. In Fig. 18, a vertical displacement of the

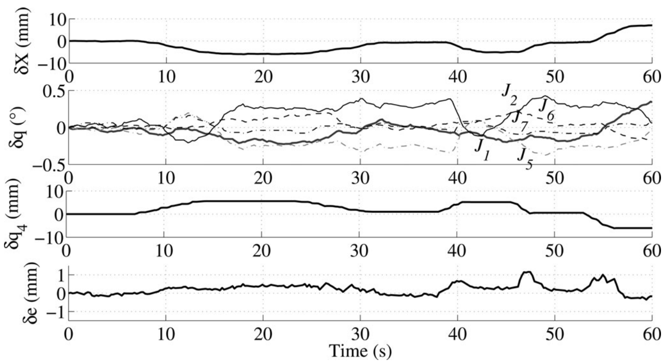

Fig. 18. Motion compensation: example of a vertical movement δX of the phantom head. The joint variations δq are represented as well as the variation of the position error δe.

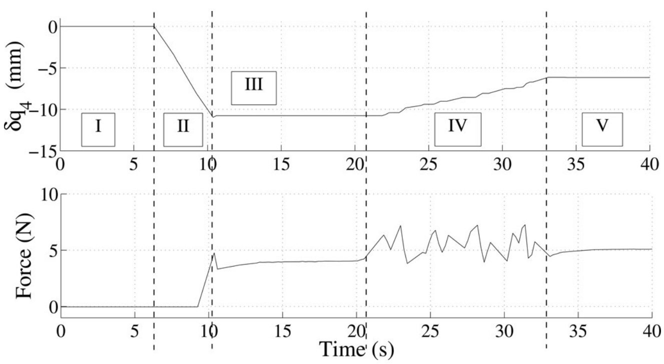

Fig. 19. Evaluation of the force control by simulating the head contact on the coil surface of contact.

head recorded by the Polaris is represented. The corrections of the joint values and the variation of the position error of the coil with respect to the head are represented as well. The error variation remains below 1 mm during the experiment.

C. Force Control

The force control is evaluated by recording the force measured with the piezoresistive sensors during a contact simulated by touching the coil surface. In Fig. 19, the phase I corresponds to the position control of the joint J4. After 7 s, the force control is started. The reference force value is obtained after a 3-s transient period. The value remains constant in the absence of movement during the phase III. During the phase IV, the head is moved to observe how the joint J4 position is modified to keep the contact force close to the reference value. After a 5-mm displacement, the contact force value in phase V is roughly equal to the value during phase III.

D. Discussion

The level of repeatability obtained with this first prototype is very promising. The standard deviation is indeed close to the one of the Polaris measuring device that is used in this evaluation. A first interest of the robotization of TMS appears: the repeatability of the coil positioning task is high and does not depend on human factors such as the experience of an operator.

In terms of accuracy, the level of performance obtained with the prototype is interesting even though slightly limited, with a mean tangential error equal to 5 mm. Further experiments have shown that the kinematics of the wrist do not exactly correspond to the kinematic model of the structure due to manufacturing and assembly imperfections. The corresponding position errors cannot be suppressed easily even with a calibration. With an improved wrist design, the accuracy should be significantly improved. The proposed correction strategy appears also very efficient to correct this problem. By identifying the errors in a first step, before the stimulation session, the position errors are divided by two after correction. The accuracy improvement occurs even if the subject is only approximately centered in the mechanism. The current design, thus, provides a level of performance that is already very satisfying for medical investigation.

The tangential errors, that represent an error in the definition of the stimulated point, can be lowered by open-loop control with correction of the kinematic errors. Using the Polaris to get a closed-loop control, these errors can even decrease to values comparable to the accuracy of the Polaris device. On the contrary, the normal error cannot be suppressed. Further experiments have shown that the head registration can introduce significant errors. A point located on the reconstructed head may be unreachable because it is located beneath the head of the subject after registration. Another reason lies in the geometry of the coil. The coil plane of contact cannot always be positioned correctly for any point on the head as detailed in Section V-B1. Depending on the actual geometry of the head, the plane of the coil can come into contact with the head at a location which is not the center of the coil. This can happen, for instance, for portions of the head that are not locally convex. Such errors are related to the stimulation definition and the stimulation coil geometry, but not related to the robotic system itself.

The improvement of TMS provided by the motion compensation and force control is clearly outlined by the experimental results. When the head moves slowly, the variation of the position error remains in the order of 1 mm. At the same time, the force control of the coil allows us to keep the force applied on the subject's head at a level which is compatible with the safety and the comfort of the subject. This also means that the subject does not have to be constrained during the treatment, which improves his/her comfort. The use of the robotic system also opens the possibility of delivering stimulation along continuous paths with a high level of accuracy in order to investigate new stimulation techniques.

VII. Conclusion

TMS possesses a great potential in the investigation and treatment of several pathologies. Introducing robotics for TMS appears natural to solve the limitations of manual procedures in terms of difficulty and accuracy. In this paper, we have proposed a dedicated robotic system and its associated workflow to ensure a high level of accuracy and safety.

Safety is taken into account at the hardware and software levels. From a hardware point of view, the robot architecture is designed to suppress any risk of interference between the robot and the patient. The unique robot kinematics allows us also to perform the force control of the coil with only one degree of freedom, thanks to a direct measurement of the contact force. During the integration, the power, velocity, and maximum torque of the actuators have been minimized to limit risks, even in case of control failure. A specific design has been adopted for the second joint that allows the subject to exit easily from the system even in case of power failure. From a software point of view, the dynamics of the force control and motion compensation are restricted so that the robotic arm cannot perform dangerous motions for the patient.

Motion compensation and contact force control have experimentally proved their efficiency. The first prototype of the proposed robotic system already provides levels of repeatability and accuracy that open new perspectives in the development of TMS. In the future, it will be interesting to further analyze the potential influence of the robotic system on the properties of the magnetic field generated by the coil. First results with a protocol such as motor cortex cartography do not show significant modification of the stimulation, but this has to be confirmed. Future work also includes a quantitative comparison of robotic and manual techniques, with or without navigation tools. Investigation on healthy subjects and patients will then be considered to evaluate more accurately the medical benefits.

Acknowledgment

The authors would like to thank R. Ginhoux and B. Maurin from Axilum Robotics for their support in the implementation of the control of the robotic system and in the experimental evaluation.

References

[1] A. T. Barker, R. Jalinous, and I. L. Freeston, "Non-invasive magnetic stimulation of human motor cortex," *The Lancet*, vol. 325, no. 8437, pp. 1106–1107, 1985.

[2] J. O'Reardon, H. Solvason, P. Janicak, S. Sampson, K. Isenberg, Z. Nahas, W. McDonald, D. Avery, P. Fitzgerald, C. Loo, M. Demitrack, M. George, and H. Sackeim, "Efficacy and safety of transcranial magnetic stimulation in the acute treatment of major depression: A multisite randomized controlled trial," *Biol. Psychiatry*, vol. 62, pp. 1208–1216, 2007.

[3] A. Gershon, P. Dannon, and L. Grunhaus, "Transcranial magnetic stimulation in the treatment of depression," *Amer. J. Psychiatry*, vol. 160, no. 5, pp. 835–845, 2003.

[4] R. Hoffman, K. Hawkins, R. Gueorguieva, N. Boutros, F. Rachid, K. Carroll, and J. Krystal, "Transcranial magnetic stimulation of left temporoparietal cortex and medication-resistant auditory hallucinations," *Archives General Psychiatry*, vol. 60, pp. 49–56, 2003.

[5] G. Giuponni, R. Pycha, B. Dell'Osso, M. Pompili, M. Walpoth, A. Hausmann, J. D. Pauli, A. Erfurth, and A. Conca, "Neurophysiological and neuropsychiatric aspects of transcranial magnetic stimulation," *Clin. Neuropsychatry*, vol. 6, pp. 234–245, 2009.

[6] U. Herwig, F. Padberg, J. Unger, M. Spitzer, and C. Schonfeldt-Lecuona, "Transcranial magnetic stimulation in therapy studies: Examination of the reliability of standard coil positioning by neuronavigation," *Biol. Psychiatry*, vol. 50, pp. 58–61, 2001.

[7] S. Lisanby, L. Kinnunen, and M. Crupain, "Applications of TMS to therapy in psychiatry," *J. Clin. Neurophysiol.*, vol. 19, pp. 344–360, 2002.

[8] R. Ahdab, S. Ayache, P. Brugieres, C. Goujon, and J.-P. Lefaucheur, "Comparison of "standard" and "navigated" procedures of TMS coil positioning over motor, premotor and prefrontal targets in patents with chronic pain and depression," *Clin. Neurophysiol.*, vol. 40, pp. 27–36, 2010.

[9] R. Sparing, D. Buelte, I. Meister, T. Paus, and G. Fink, "Transcranial magnetic stimulation and the challenge of coil placement: A comparison of conventional and stereotaxic neuronavigational strategies," *Human Brain Mapping*, vol. 28, pp. 82–96, 2008.

[10] U. Herwig, C. Schonfeldt-Lecuona, A. Wunderlich, C. von Tiesenhausena, A. Thielscher, H. Walter, and M. Spitzera, "The navigation of transcranial magnetic stimulation," *J. Psychiatric Res.*, vol. 108, pp. 123–131, 2001.

[11] S. Neggers, T. Langerak, D. Schutter, R. Mandl, N. Ramsey, P. Lemmens, and A. Postma, "A stereotactic method for image-guided transcranial magnetic stimulation validated with fMRI and motor-evoked potentials," *Neuroimage*, vol. 21, pp. 1805–1817, 2004.

[12] J. Lancaster, S. Narayana, D. Wenzel, J. Luckemeyer, J. Roby, and P. Fox, "Evaluation of an image-guided, robotically positioned transcranial magnetic stimulation system," *Human Brain Mapping*, vol. 22, pp. 329–340, 2004.

[13] S. R. Kantelhardt, T. Fadini, M. Finke, K. Kallenberg, J. Siemerkus, V. Bockermann, L. Matthaeus, W. Paulus, A. Schweikard, V. Rohde, and A. Giese, "Robot-assisted image-guided transcranial magnetic stimulation for somatotopic mapping of the motor cortex: A clinical pilot study," *Acta. Neurochirurgica*, vol. 152, pp. 333–343, 2010.

[14] X. Yi and R. Bicker, "Design of a robotic transcranial magnetic stimulation system," presented at the IEEE Conf. Robot., Autom. Mechatronics, Singapore, 2010.

[15] E. Dombre, G. Duchemin, P. Poignet, and F. Pierrot, "Dermarob: A safe robot for reconstructive surgery," *IEEE Trans. Robot. Autom.*, vol. 19, no. 5, pp. 876–884, Oct. 2003.

[16] R. Taylor and D. Stoianovici, "Medical robotics in computer-integrated surgery," *IEEE Trans. Robot. Autom.*, vol. 19, no. 5, pp. 765–781, Oct. 2003.

[17] C. Lebossé, P. Renaud, B. Bayle, M. de Mathelin, O. Piccin, E. Laroche, and J. Foucher, "Robotic image-guided transcranial magnetic stimulation," presented at the Proc. Comput. Assisted Radiology Surgery, Osaka, Japon, 2006.

[18] C. Lebossé, P. Renaud, B. Bayle, M. de Mathelin, and J. Foucher, "A robotic system for automated image-guided transcranial magnetic stimulation," in *Proc. 3rd IEEE-NIH Life Sci. Syst. Appl. Workshop*, Bethesda, MD, 2007, pp. 55–58.

[19] *Polaris System*, NDI. (2011). [Online]. Available: Link: http://www.ndigital.com/medical/polarisfamily.php

[20] U. Mosimann, S. Marre, S. Werlen, W. Schmitt, C. Hess, H. Fisch, and T. Sclaepfer, "Antidepressant effects of repetitive transcranial magnetic stimulation in the elderly: Correlation between effect size and coil-cortex distance," *Arch. Gen. Psychiatry*, vol. 59, no. 6, pp. 560–561, 2002.

[21] A. Thielscher and T. Kammer, "Linking physics with physiology in TMS: A sphere field model to determine the cortical stimulation site in TMS," *Neuroimage*, vol. 17, pp. 1117–1130, 2002.

[22] T. Wagner, M. Zahn, A. Grodzinsky, and A. Pascual-Leone, "Three-dimensional head model stimulation of transcranial magnetic stimulation," *IEEE Trans. Biomed. Eng.*, vol. 51, no. 9, pp. 1586–1598, Sep. 2004.

[23] A. Zangen, Y. Roth, B. Voller, and M. Hallett, "Transcranial magnetic stimulation of deep brain regions: evidence for efficacy of the H-coil," *Clin. Neurophysiol.*, vol. 116, pp. 775–779, 2005.

[24] D. Rudiak and E. Marg, "Finding the depth of magnetic brain stimulation: A re-evaluation," *Electroencephalography clin. Neurophysiol.*, vol. 93, pp. 358–371, 1994.

[25] C. Hovey and R. Jalinous, *The guide to magnetic stimulation*, Magstim, Whitland, U.K. 2006 [Online]. Available: Link: http://www.magstim.com/downloads/guidesandreview.html

[26] C. Lebossé, "Stimulation magnétique transcrânienne robotisée guidée par imagerie médicale" Ph.D. dissertation, Strasbourg Univ., Strasbourg, France, 2008.

[27] R. Motmans, *Body dimensions of the Belgian population*, Dinbelg, Amsterdam, The Netherlands, 2005 [Online]. Available: Link: http://www.dinbelg.be/anthropometry.htm

[28] K. Manjunath, "Estimation of cranial volume in dissecting room cadavers," *J. Anatomical Soc. India*, vol. 51, no. 5, pp. 168–172, 2002.

[29] M. Carricato and V. Parenti-Castelli, "A novel fully decoupled two-degrees-of-freedom parallel wrist," *The Int. J. Robot. Res.*, vol. 23, no. 6, pp. 661–667, 2004.

[30] S. Salcudean, W. Zhu, P. Abolmaesumi, S. Bachmann, and P. Lawrence, "A robot system for medical ultrasound," in *Proc. 9th Int. Symp. Robot. Res.*, 1999, pp. 152–159.

[31] T. Yoshikawa, "Manipulability of robotic mechanisms," *Int. J. Robot. Res.*, vol. 4, no. 2, pp. 3–9, 1985.

[32] Y. Nakamura, *Advanced Robotics: Redundancy and Optimization*. Boston, MA: Addison-Wesley, 1991.

[33] A. Cavelaars, A. Kunst, J. Geurts, R. Crialesi, L. Grotvedt, and U. Helmert, “Persistent variations in average height between countries and between socio-economic groups: An overview of 10 european countries,” *Ann. Human Biology*, vol. 27, no. 4, pp. 407–421, 2000.
[34] C. Lebossé, P. Renaud, B. Bayle, and M. de Mathelin, “Modeling and evaluation of low-cost force sensors,” *IEEE Trans. Robot.*, vol. 27, no. 4, pp. 815–822, Aug. 2011.
[35] K. S. Arun, T. S. Huang, and S. D. Blostein, “Least squares fitting of two 3d point sets,” *IEEE Trans. Pattern Anal. Mach. Intell.*, vol. 9, no. 5, pp. 698–700, 1987.
[36] *TMS Navigator*, Localite. (2011) [Online]. Available: Link: http://www.localite.de/en/tms
[37] G. Oriolo, M. Ottavi, and M. Venditelli, “Probabilistic motion planning for redundant robots along given end-effector paths,” in *Proc. IEEE Int. Conf. Intell. Robot. Syst.*, Lausanne, Switzerland, 2002, vol. 2, pp. 1657–1662.
[38] L. Kavraki, P. Švestka, J.-C. Latombe, and M. Overmars, “Probabilistic roadmaps for path planning in high-dimensional configuration spaces,” *IEEE Trans. Robot. Autom.*, vol. 12, no. 4, pp. 566–580, Aug. 1996.

Lucile Zorn received the Mechatronics Eng. degree from the Institut National des Sciences Appliquées, Strasbourg, France, and the M.Sc. degree in robotics from the University of Strasbourg, Strasbourg, in 2008.

Since 2008, she has been a Research Engineer with the University of Strasbourg, where she is a member of the Control, Vision, and Robotics Team, Laboratoire des Sciences de l’Image, de l’Informatique et de la Télédétection. Her research interests include medical robotics and mechanical design.

Pierre Renaud received the M.Sc. degree in mechanics and materials from the ENS Cachan, Cachan, France, in 2000, and the Ph.D. degree in robotics from the Clermont-Ferrand University, Clermont-Ferrand, France, in 2003.

Since 2004, he has been an Associate Professor at Institut National des Sciences Appliquées, Strasbourg, France, and member of the EAVR team at the Laboratoire des Sciences de l’Image, de l’Informatique et de la Télédétection, University of Strasbourg, Strasbourg, France. He is the Co-Founder of Axilum Robotics, a spin-off dedicated to the development of robotized magnetic transcranial procedures. His research interests include medical robotics, robot design, parallel robots, and mechatronics.

Bernard Bayle received the agrégation in electrical engineering from the Ecole Normale Supérieure de Cachan, Cachan, France, in 1995, and the M.Sc. and Ph.D. degrees in control theory and robotics from the University of Toulouse (LAAS-CNRS), Toulouse, France, in 1996 and 2001, respectively. He became a Lecturer at the Ecole Nationale Supérieure de Physique de Strasbourg (ENSPS), University of Strasbourg, Strasbourg, France, in 2002, where he has created the ICTs & healthcare curriculum. He has been a Professor at ENSPS since 2011. He is a member of the Automation, Vision and Robotics research group of the Laboratoire des Sciences de l’Image, de l’Informatique et de la Télédétection, University of Strasbourg. He is the coordinator for medical robotics at CNRS Robotics Research Group. He is the Co-Founder of Axilum Robotics, a spin-off dedicated to the development of robotized magnetic transcranial procedures. His research interests include design, modeling, and control of robotic systems, with a focus on medical robotics and force feedback technologies.

Laurent Goffin received the M.Sc. degree in medical computer science from the University Pierre et Marie Curie, Paris, France, in 2000.

From 2000 to 2001, he was a Research Engineer at the ChIR team at the Institut National de Recherche en Informatique et en Automatique, Sophia Antipolis, France. He worked five years on biomedical softwares in the VirtualS team at the Institut de Recherche contre le Cancer de l’Appareil Digestif, Strasbourg, France. Since 2010, he has been working with the Control, Vision and Robotics Team at Laboratoire des Sciences de l’Image, de l’Informatique et de la Télédétection, University of Strasbourg, Strasbourg. His research interests include augmented reality, computer vision, and robotics.

Cyrille Lebossé received the Electrical Engineering degree from the Ecole Nationale Supérieure de Physique de Strasbourg (ENSPS), University of Strasbourg, Strasbourg, France, in 2004, and the Ph.D. degree in medical robotics and computer vision from the University Louis Pasteur, Strasbourg, in 2008.

Since 2008, he has been a Research and Development Engineer for Luxscan Technologies, Ehlerange, Luxembourg. His current research interests include computer vision, image processing, and vision systems design.

Michel de Mathelin received the Electrical Engineering degree from Louvain University, Louvain-La-Neuve, Belgium, in 1987 and the M.Sc. and Ph.D. degrees in electrical and computer engineering from the Carnegie Mellon University, Pittsburgh, PA, in 1988 and 1993, respectively.

During 1991–1992, he was a Research Scientist in the Department of Electrical Engineering, Polytechnic School of the Royal Military Academy, Brussels, Belgium. In 1993, he became Assistant Professor at the University of Strasbourg, Strasbourg, France. Since 1999, he has been a Professor at the Ecole Nationale Supérieure de Physique de Strasbourg, University of Strasbourg, Strasbourg, France, where he is also the Head of the Automation, Vision and Robotics Research Group in the Laboratoire des Sciences de l’Image, de l’Informatique et de la Télédétection. He is the Co-Founder of Axilum Robotics, a spin-off dedicated to the development of robotized magnetic transcranial procedures. His current research interests include medical robotics, visual servoing, adaptive, and robust control.

Dr. de Mathelin has been an Associate Editor of the IEEE CONTROL SYSTEM TECHNOLOGY With his coauthors, he received the ICRA 2004 Best Vision Paper Award and the 2005 King-Sun Fu Memorial Best IEEE Transactions on Robotics Paper Award. He is a fellow of the Belgian American Educational Foundation.

Jack Foucher has received certificate in the fields of biochemistry and neurochemistry during his medical training started in 1986 and became a specialist in the field of neurology and neurophysiology between 1996 and 2001. In 2001, he presented his thesis titled “Functional Cerebral Integration: Concepts and Methods.” He received the Ph.D. degree from Louis Pasteur University, Strasbourg, France, in 2007, with his thesis titled “Functional Cerebral Integration Disorders in Schizophrenia.”

He is currently with Department of Psychiatry, University Hospital of Strasbourg, Strasbourg, France. He is involved in psychiatry and clinical physiology service in the field of psychotic disorders. His research interests include the study on methodological development of multimodal imaging (EEG, MEG, IRMf, TMS) and the treatment with rTMS.

Dr. Foucher has received with Conseil General du Bas-Rhin Thesis Prize.